



Studies of the triplet state of the proton-transfer tautomer in salicylaldehydes

Pi-Tai Chou ^{a,*}, Chau-Shuen Chiou ^b, Wei-Shan Yu ^b, Guo-Ray Wu ^b,
Tai-Huei Wei ^c

^a Department of Chemistry, National Taiwan University, Taipei 621, Taiwan, ROC

^b Department of Chemistry, The National Chung-Cheng University, Chia Yi, Taiwan, ROC

^c Department of Physics, The National Chung-Cheng University, Chia Yi, Taiwan, ROC

Received 1 August 2002

Abstract

The spectroscopy and dynamics of the low-lying triplet state of the proton-transfer tautomer in salicylaldehydes have been studied via internal heavy-atom effects coupled with a sensitive near-IR detecting system. For 3,5-diiodosalicylaldehyde a weak proton-transfer keto-tautomer phosphorescence was resolved with a maximum at 710 nm ($\tau_p \sim 1.8 \mu\text{s}$, $\Phi_{\text{obs}} \sim 5.23 \times 10^{-4}$) in a 77 K methylcyclohexane glass. The results, in combination with the time-resolved thermal lensing experiment, further deduced the triplet-state population yield and radiative decay rate to be 0.20 (298 K) and $3.12 \times 10^2 \text{ s}^{-1}$, respectively. Consequently, the energetics and dynamics of the triplet states during a proton transfer cycle are discussed in detail.

© 2003 Elsevier Science B.V. All rights reserved.

1. Introduction

The fundamental approach to a proton transfer process, which is crucial to many chemical and biological reactions, has relied deeply on studies of the excited state intramolecular proton transfer (ESIPT) reaction [1–5]. The ESIPT reaction generally incorporates transfer of a hydroxyl (or amino) proton to the carbonyl oxygen (or pyridinic nitrogen) through a preexisting hydrogen bonding (HB) configuration. The resulting proton-

transfer tautomer possesses vast differences in structure and electronic configuration from its corresponding normal species. Accordingly, a large Stokes shifted $S'_1 \rightarrow S'_0$ fluorescence (hereafter, the prime sign denotes the proton-transfer tautomer) was observed. This unusual photo-physical property has found many important applications. Prototypical examples are probes for solvation dynamics [6] and biological environments [7], the development of laser dyes [8,9], ultraviolet stabilizers [10], metal ion sensors [11] and radiation hard-scintillator counters [12], etc.

In contrast to extensive efforts made on the singlet manifold, studies on the spectroscopy and dynamics of triplet states in ESIPT molecules are

* Corresponding author. Fax: +886-2-23695208.

E-mail address: chop@ccms.ntu.edu.tw (P.-T. Chou).

relatively rare. Disregarding the first case of the ESIPT reaction on methyl salicylate reported in as early as 1956 [13], only recently has the investigation of $T_1' \rightarrow S_0'$ phosphorescence become possible. Grellmann and co-workers [14,15], first observed the $T_1' \rightarrow S_0'$ phosphorescence in 2-(2'-hydroxyphenyl)benzoxazole. Subsequently, Chou et al. [16] reported the weak 648 nm phosphorescence of 2-(2'-hydroxyphenyl)-benzothiazole (HBT) in a 77 K hydrocarbon glass. Grabowska et al. [17] then examined another case of proton-transfer phosphorescence in 2,2'-bipyridyldiol systems. Recently, Catalán and Diaz [18] applied a spin-orbit perturbation technique, i.e., the intermolecular and/or intramolecular 'heavy-atoms' effects, to achieve a feasible method of observing the desired $T_1' \rightarrow S_0'$ phosphorescence for halogenated methylsalicylates.

The $T_1'-S_0'$ energy gap in the above few cases is usually restricted to the visible region (<700 nm). For those ESIPT molecules in which the $T_1'-S_0'$ energy gap is expected to be in the far visible region extending to the near-infrared (NIR) region (<15 000 cm^{-1}), the spectrally resolved $T_1' \rightarrow S_0'$ phosphorescence was obscure. One major obstacle for detecting the NIR phosphorescence is the dominant $T_1' \rightarrow S_0'$ radiationless deactivation process. When the energy gap decreases, the forbidden triplet \rightarrow singlet radiative decay rate constant be-

comes smaller [19]. Conversely, the rate of the radiationless deactivation pathway is expected to increase [20], in particular for ESIPT molecules where the vibrational modes associated with intramolecular hydrogen bonds usually act as good quenchers for the emission [21]. One would thus expect that in the condensed phase, the lowest-lying tautomer triplet state in NIR might give rise to an extremely low yield of phosphorescence.

Very recently, we have reported the spectroscopy and dynamics of the proton-transfer tautomer 735-nm phosphorescence for 7,9-diiodo-10-hydroxybenzo[*h*]quinoline. The results, in combination with the triplet-state sensitizing singlet oxygen experiment, led us to deduce relative energetics in different spin manifolds during a proton-transfer reaction [22]. To further extend the approach on the spectroscopy and dynamics of triplet states in other ESIPT systems, we have investigated salicylaldehyde (SA) and its halogenated derivative 3,5-diiodosalicylaldehyde (DISA) in the triplet manifold. SA is structurally the simplest aromatic ESIPT system, of which the physical properties in the singlet-state manifold are readily accessible to both spectroscopic and theoretical analyses. In the electronic ground-state SA exists dominantly in an enol form (conformer E, see Fig. 1) possessing an intramolecular hydrogen bond between hydroxyl and carbonyl groups [23–25]. Our approach to achieve

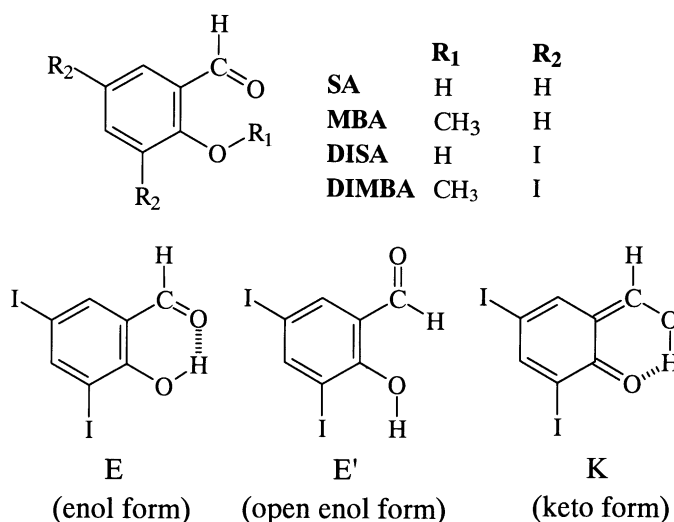


Fig. 1. Structures of SA and DISA and their corresponding methyl derivatives.

the feasibility of detecting the ultraweak phosphorescence is based on two key factors; namely the intramolecular heavy-atom effect coupled with an ultrasensitive NIR detection system. In this study, we have further applied a time-resolved thermal lensing technique to directly monitor the population yield of the triplet state. The results lead to the establishment of energetics for DISA in different spin manifolds during a proton-transfer cycle.

2. Experimental

2.1. Material

Salicylaldehyde (SA, Riedel-de Haën, 99%) was purified by vacuum distillation in the grease-free condition. 3,5-Diiodosalicylaldehyde (DISA, Lancaster, 98%) was purified by column chromatography (eluent CH_2Cl_2) until a single spot showed on the TLC plate. The purity was checked by ^1H NMR and fluorescence excitation spectrum. 2-Methoxybenzaldehyde (MBA) was synthesized by the methylation of SA in basified methyl iodide solution. 3,5-Diiodo-2-methoxybenzaldehyde (DIMBA) was then synthesized by adding a solution containing MBA (0.01 mol) and glacial acetic acid (4 ml) in chloroform (10 ml) to a solution of iodine (0.02 mol in 20 ml methanol) for a period of 1 h. The precipitate was collected and neutralized with sodium carbonate to give DIMBA. Methylcyclohexane (MCH, Aldrich) was of spectrograde quality and used without further purification.

2.2. Method

Detailed steady state, time-resolved and quantum yield measurements of fluorescence and phosphorescence have been elaborated in previous reports [22,26]. The nanosecond transient absorption was recorded by a laser flash photolysis system (Edinburgh LP920), in which an Nd:YAG laser (355 nm) pumped optical parametric oscillator and a white-light square pulse were used as pump and probe beams, respectively. These two pulses were crossed at a 90° angle with an overlapping distance of ~ 10 mm. The temporal resolution was limited by the excitation pulse duration of ~ 8 ns.

The time-resolved thermal lensing (TRTL) technique [27] was applied to measure the radiationless decay dynamics. Briefly, the TRTL setup consists of an Nd:YAG laser (355 nm) of which the output energy can be finely adjusted through a dual- $\lambda/2$ -plates configuration. A He–Ne laser (JDS Uniphase 1125; 632.8 nm, 5 mW) equipped with a stabilized power supply was used as an analyzing beam for TRTL signals. The He–Ne beam was focused in front of the sample cell with an $f = 30$ mm lens, and was in a direction of 180° with respect to the Nd:YAG excitation beam (focused by a $f = 200$ mm lens). The He–Ne laser beam after the sample cell was passed through a pinhole (Corion 2401; 300 μm diameter) and a set of filters combination. The beam intensity was then detected with a photomultiplier tube (Hamamatsu R943), of which the output signals were converted into the voltage (Tektronix TDS 3054; 5GS/Sampling). The system response is limited by the acoustic transient time defined by w_p/v_s , where w_p is the radius of the waist of the pump beam at the focal point and was measured to be ~ 60 μm in our current setup, v_s denotes the speed of sound in the solvent, which is 1.28×10^3 m/s in MCH. This gives a system response time of ~ 50 ns in MCH.

3. Results and discussion

3.1. Absorption and fluorescence properties

The room-temperature absorption and emission spectra of DISA in MCH are shown in Fig. 2. The $S_0 \rightarrow S_1$ ($\pi\pi^*$) absorption exhibits an onset at ~ 400 nm with a band maximum at 360 nm ($\epsilon_{360} \sim 3600 \text{ M}^{-1} \text{ cm}^{-1}$). The fluorescence is characterized by a single emission band maximum at 560 nm ($\Phi_f \sim 2.3 \times 10^{-3}$) with a lifetime measured to be ~ 52 ps. The normal Stokes shifted fluorescence expected to be in the region of 350–450 nm was not detected. The excitation spectrum of the 560-nm band is independent of the monitored emission wavelength and is effectively identical with the absorption profile. In comparison, DIMBA, which is considered a non-proton-transfer model with a similar electronic configuration to DISA, exhibited

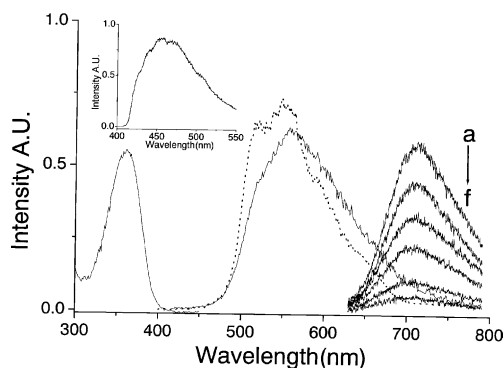


Fig. 2. Absorption and emission spectra of DISA in MCH at 298 (—) and 77 K (---). (a)–(f): The time dependent spectral evolution of the phosphorescence for DISA (5.7×10^{-5} M) in a 77 K MCH glass at >600 nm with a delay time of (a) 200 ns, (b) 800 ns, (c) 1.6 μ s, (d) 2.4 μ s, (e) 4.7 μ s and (f) 6.2 μ s. Inset: the appearance of the E' phosphorescence after 355-nm (5 mJ/pulse) irradiation for 5 min in a 77 K MCH glass.

a very weak, normal Stokes shifted fluorescence maximized at ~ 400 nm (see Table 1). Accordingly, the ~ 560 nm emission band with a Stokes shift of as large as 9920 cm^{-1} (peak-to-peak) measured in DISA is unambiguously ascribed to the keto-tautomer (K, see Fig. 1) fluorescence resulting from ES IPT.

3.2. Photophysics of the triplet state

Fig. 3 depicts the room-temperature transient absorption spectra of DISA in the degassed MCH. The transient absorption maximized at 420 nm undergoes a fast single exponential decay rate of

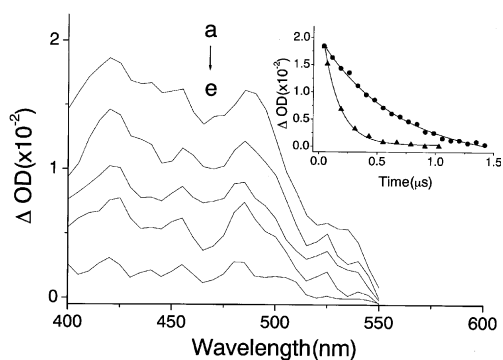


Fig. 3. Temporal evolution of the transient absorption spectra of DISA in degassed MCH (298 K) with a delay time of (a) 130 ns, (b) 350 ns, (c) 500 ns, (d) 750 ns and (e) 1.2 μ s. Inset: the plot of 420-nm absorption intensity versus various delay times in degassed (●) and aerated (▲) solution.

1.5×10^6 s^{-1} ($\tau = 0.67$ μ s), of which the relaxation dynamics were significantly quenched by O_2 . As shown in the inset of Fig. 3, the decay rate was increased to $\sim 7.0 \times 10^6$ s^{-1} in the aerated MCH ($\text{O}_2 \sim 2.3 \times 10^{-3}$ M). On the basis of the Stern–Volmer plot (not shown here), an O_2 quenching rate constant of 2.4×10^9 s^{-1} was extracted, which within experimental error is equal to 1/9 diffusion-controlled rate ($\sim 3.0 \times 10^9$ M^{-1} s^{-1} in MCH [28]) theoretically derived from the triplet (T)- O_2 sensitization. Thus, the assignment of the observed transient absorbance in DISA to the triplet–triplet transition is unambiguous. In a comparative study, the transient absorption of DIMBA in degassed MCH was also performed, of which both

Table 1
Photophysical properties of SA, DISA and DIMBA in MCH at 298 and 77 K

	Absorption	Fluorescence			Phosphorescence ^a		
	λ_{max} (nm)	λ_{max} (nm)	Φ_{obs}	τ_{f} (ps)	λ_{max} (nm)	Φ_{obs}	τ_{p} (s)
SA	330	510	1.0×10^{-3}	50	435 ^b	–	1.3×10^{-3}
		505 ^a	$1.3 \times 10^{-2, a}$	467 ^a			
DISA	360	560	2.3×10^{-3}	52	710	5.2×10^{-4}	1.8×10^{-6}
		550 ^a	$9.1 \times 10^{-3, a}$	240 ^a	455 ^b	–	3.6×10^{-4}
		420 ^{b, c}	–	–	–	–	–
DIMBA	352	$\sim 400^c$	–	–	445	2.2×10^{-2}	2.8×10^{-4}

^a 77 K.

^b The photolysis product at 77 K.

^c Emission is too weak to perform dynamic and quantum yield measurements.

spectral feature ($\lambda_{\max} \sim 470$ nm) and dynamics of decay ($t_{1/2} \sim 20$ μ s) are considerably different from those of DISA. Since DIMBA represents a non-proton-transfer model, the assignment of triplet–triplet transient absorption originating from the enol conformer is obvious. Accordingly, the 420-nm transient absorption in DISA is tentatively ascribed to the triplet–triplet absorption of the keto-tautomer (i.e., conformer K) species.

Caution has to be taken in performing phosphorescence measurements in the low-temperature solid matrices. Nagaoka et al. [23] have reported that except for the major channels of radiationless deactivation (i.e., proton transfer reaction, internal conversion, etc.), SA undergoes a minor photoisomerization channel, forming an open-form conformer trapped in the cold, solid matrices. Morgan et al. [25] further resolved the open conformer by FTIR analyses of vibrational modes for various deuterium isotope substitutions, and concluded that in the open-form conformer both hydroxyl and aldehyde functional groups rotate by 180° . For DISA, the formation of a similar open-form conformer (E' , see Fig. 1) was observed in the 77 K MCH glass matrices (vide infra). Such an interference may hamper our goal of detecting the $T'_1 \rightarrow S'_0$ phosphorescence. Fortunately, the open-form product can be experimentally avoided by taking a few laser shots during the data acquisition accompanied by a low power of excitation ($\ll 0.5$ mJ/cm²), while spectra could still be obtained with a good signal-to-noise ratio due to the highly sensitive detecting system.

Under low-excitation energy, DISA exhibit unique keto-tautomer fluorescence maximized at 550 nm ($\tau_f \sim 240$ ps) in 77 K MCH glassy matrices (Fig. 2). In order to obtain the presumably ultra-weak phosphorescence attributed to the $T'_1 \rightarrow S'_0$ transition of the proton-transfer tautomer, the gate of intensified charge coupled detector (ICCD [22]) was opened at a delay time of ~ 50 ns to eliminate the keto-tautomer fluorescence. On the other hand, due to its relatively much longer lifetime of ~ 0.36 ms, the interfering phosphorescence resulting from the open conformer (E' , vide infra), if there is any, can be eliminated by gating ICCD with a window as small as 200 ns. Under these experimental conditions an attempt to detect the

keto-tautomer phosphorescence of SA in a 77 K MCH glass failed. In contrast, a long-lived emission maximum at 710 nm was apparently resolved for DISA (Fig. 2). The relaxation dynamics can be well fitted by single exponential decay kinetics with a lifetime of 1.8 μ s. Similar excitation spectra (not shown here) between monitoring at tautomer fluorescence (i.e., the 550-nm emission) and the 710-nm phosphorescence concluded that both emission bands originate from a common ground-state species, i.e., conformer E. For comparison, DIMBA in a 77 K MCH glass exhibits an enol phosphorescence maximum at ~ 445 nm ($\tau_p \sim 0.28$ ms, see Table 1) of which both spectral feature and relaxation dynamics are quite different from those of DISA. Thus, the 710-nm emission in DISA can be unambiguously ascribed to the $T'_1 \rightarrow S'_0$ phosphorescence of the keto-tautomer.

Two close lying $^1n\pi^*$ and $^1\pi\pi^*$ states (<3 kcal/mol) have been reported for SA [25,29], in which the photoinduced $E \rightarrow E'$ rotamerization originates from the lowest singlet excited state possessing a $^1n\pi^*$ configuration [29]. For DISA, induced by the diiodo-substitution, the first $^1\pi \rightarrow \pi^*$ absorption maximum of 360 nm is ~ 2500 cm⁻¹ red shifted relative to that of SA ($\lambda_{\max} \sim 330$ nm, see Table 1). It is thus reasonable to predict a reverse energetics between $^1n\pi^*$ and $^1\pi\pi^*$ states in DISA. Accordingly, the rotamerization efficiency should be significantly reduced due to the competing fast $^1n\pi^* \rightarrow ^1\pi\pi^*$ internal conversion. Support of this viewpoint is given by the lack of resolving any oxygen-independent transient absorption associated with the E' conformer. Nevertheless, a non-negligible photoinduced rotamerization process still takes place, of which the product (e.g., the E' form) can be trapped and accumulated for further analyses in the 77 K MCH glass matrices. Inset of Fig. 2 shows the 455-nm phosphorescence spectrum of the photolysis product of DISA under high laser intensity (>5 mJ/cm²). Both spectral and dynamic ($\tau \sim 0.36$ ms) features of the 455-nm phosphorescence are similar to that of the 445-nm phosphorescence observed in DIMBA. This, in combination with the reversibility of the reaction during a thawing/freezing cycle, led us to conclude the 455-nm phosphorescence originate from a non-

hydrogen-bonded enol form, possibly the E' conformer. Because this issue is not the main focus of this study, further quantitative elaboration has not been pursued.

3.3. TRTL experiments

Previously, we made an attempt to quantify the triplet-state yield through a triplet-state sensitizing $^1\text{O}_2$ experiment [22]. This method is valid only if the efficiency of $\text{O}_2(^1\Delta_g)$ sensitized by the triplet state is known. Unfortunately, this value varies with sensitizers and is rather complex to deduce. For simplicity of derivation the $^1\text{O}_2$ sensitization efficiency is generally assumed to be unity. Accordingly, this indirect method may be subject to a great deal of uncertainty. Alternatively, a TRTL technique has been developed in this study to directly quantify the yield of triplet state for DISA. For the case of DISA, the rates for both proton transfer and keto-tautomer fluorescence are fast, as indicated by the system response limited rise (<15 ps) and ~ 52 ps lifetime of the keto-tautomer emission. Furthermore, supported by the identical temporal evolution of transient absorption spectra (vide supra), it is reasonable to conclude that except for the triplet-state species, there are no other resolvable, long-lived transient species existing during a proton transfer cycle. Consequently, the rate of $\text{K} \rightarrow \text{E}$ ground-state reverse proton transfer for DISA is concluded to be faster than the system response of ~ 8 ns. Since TRTL is limited by the acoustic transient time which is ~ 50 ns in MCH in this study (see Section 2), the only slow, resolvable transient signal should originate from the triplet state. Other relaxation pathways during the proton transfer cycle should reveal instant, acoustic-transient-time limited rise kinetics.

Fig. 4 reveals the TRTL time profile of DISA in MCH. The signal apparently consists of a system irresolvable and a $0.69 \mu\text{s}$ rise component. The former is ascribed to the sum of all fast decay components, while the latter with its rise time similar to the lifetime measured from the transient absorption can thus be assigned to the decay time of the keto-tautomer triplet state. As shown in the inset of Fig. 4, the plot of the intensity of the total signal, U_t , versus the applied laser energy (5–30 μJ)

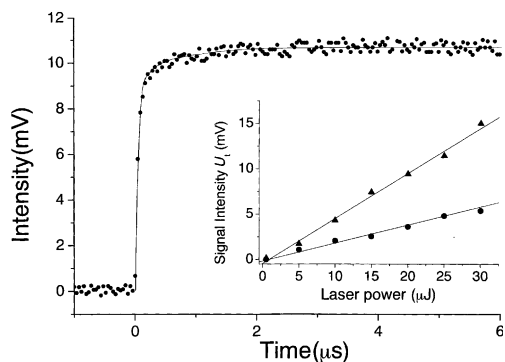


Fig. 4. The TRTL profile of DISA (1.1×10^{-4} M) in degassed MCH. Inset: the plot of total signal intensity versus 355-nm laser energies at the absorbance (355 nm) of 0.2 (●) and 0.5 (▲).

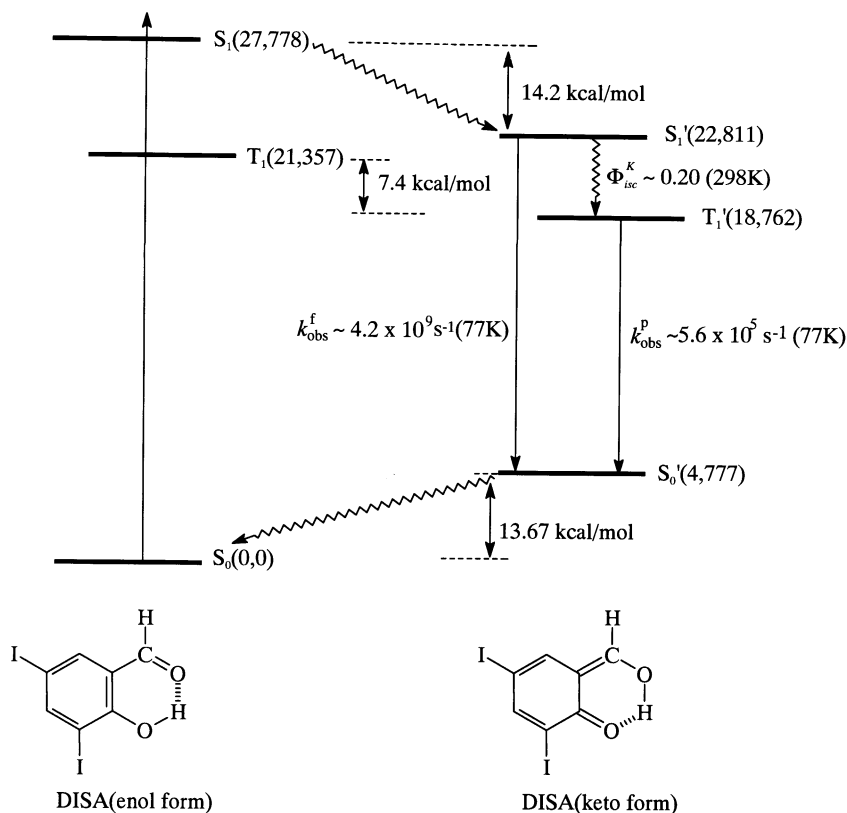
is sufficiently linear, eliminating the possibility of the multiphoton effect contributed to the TRTL signal. Since the intensity of the TRTL signal is proportional to the absolute energy dissipated, the intensity (voltage) of the slow rising signal, U_s versus U_t , can be expressed as

$$\frac{U_s}{U_t} = \frac{\Phi_{\text{pt}} \Phi_{\text{isc}}^{\text{K}} E_{\text{p}}}{\alpha E_{\text{ex}}}, \quad (1)$$

where Φ_{pt} and $\Phi_{\text{isc}}^{\text{K}}$ denote the yields of ESIPT and $\text{S}'_1 \rightarrow \text{T}'$ intersystem crossing, respectively, E_{ex} is the excitation energy, and E_{p} is the energy gap of the keto phosphorescence. α denotes the heat conversion efficiency and is equivalent to $(E_{\text{ex}} - \Phi_{\text{f}} E_{\text{s}})/E_{\text{ex}}$, where Φ_{f} and E_{s} are the quantum yield and 0–0 transition energy of the keto fluorescence. Because the yield of fluorescence Φ_{f} is as small as 2.3×10^{-3} (298 K) in DISA, α is essentially equal to 1. Due to the lack of enol fluorescence and ultrafast rise dynamics of the keto-tautomer emission, it is also reasonable to assume Φ_{pt} to be ~ 1 . E_{p} was deduced from its average energy expressed as

$$\langle E_{\text{p}} \rangle = \frac{\int I_{\text{p}}(v) v \, dv}{\int I_{\text{p}}(v) \, dv}, \quad (2)$$

where $I_{\text{p}}(v)$ denotes the relative emission intensity as a function of wavenumber. Accordingly, a value of 13985 cm^{-1} was obtained. The ratio of U_s/U_t (see Fig. 4) was calculated to be ~ 0.10 . Applying E_{ex} of 28169 cm^{-1} (355 nm) in this study, $\Phi_{\text{isc}}^{\text{K}}$ was thus deduced to be 0.2. $\Phi_{\text{isc}}^{\text{K}}$ is equivalent to $k_{\text{isc}}^{\text{K}}/k_{\text{f}}$,



Scheme 1. Relative energy levels (in cm^{-1}) and photophysical parameters for the enol and keto-tautomers of DISA estimated from either experimental or theoretical approaches. See text for the detailed description.

where k_{isc} and k_f are rate constants of intersystem crossing and the fluorescence decay, respectively, for the keto-tautomer. Knowing k_f to be $1.9 \times 10^{10} \text{ s}^{-1}$ ($\tau_f \sim 52 \text{ ps}$), k_{isc} was thus deduced to be $3.8 \times 10^9 \text{ s}^{-1}$ at 298 K.

3.4. Radiative lifetime of the keto-phosphorescence

The yield of keto-tautomer phosphorescence, $\Phi_{\text{obs}}^{\text{P}}$, was measured to be 5.23×10^{-4} in the 77 K MCH glass, which can be further expressed as

$$\Phi_{\text{obs}}^{\text{P}} = \Phi_{\text{pt}} \Phi_{\text{isc}}^{\text{K}} \Phi_{\text{p}}^{\text{K}}, \quad (3)$$

where Φ_{pt} denotes the yield of the ES IPT and is assumed to be $\sim 100\%$ efficiency at 77 K due to the irresolvable rise of the keto-tautomer fluorescence. $\Phi_{\text{p}}^{\text{K}}$ represents the intrinsic keto phosphorescence yield and is equivalent to $k_{\text{r}}^{\text{P}}/k_{\text{obs}}^{\text{P}}$ where k_{r}^{P} and $k_{\text{obs}}^{\text{P}}$,

respectively denote the radiative and measured decay rate constants of the keto phosphorescence. To obtain $\Phi_{\text{isc}}^{\text{K}}$ at 77 K, k_{isc} is further assumed to be independent of temperature. This assumption holds true if the triplet-state population proceeds only through the $S_1' \rightarrow T_1'$ intersystem crossing and the $S_1'-T_1'$ energy gap is $\gg kT$. For DISA, support for the latter assumption is given by the $>4000 \text{ cm}^{-1}$ gap measured from the difference in peak maxima between keto fluorescence ($\sim 18182 \text{ cm}^{-1}$) and phosphorescence ($\sim 14084 \text{ cm}^{-1}$). Knowing the decay rate of the keto-tautomer fluorescence to be $4.2 \times 10^9 \text{ s}^{-1}$, a value of 0.93 was estimated for $\Phi_{\text{isc}}^{\text{K}}$ in a 77 K MCH glass. As a result, $\Phi_{\text{p}}^{\text{K}}$ was deduced to be 5.62×10^{-4} . With a known $k_{\text{obs}}^{\text{P}}$ value of $5.56 \times 10^5 \text{ s}^{-1}$, the radiative decay rate of keto-tautomer phosphorescence, k_{r}^{P} , was then deduced to be $3.12 \times 10^2 \text{ s}^{-1}$.

3.5. Energetics during a proton transfer cycle

With the above spectroscopic data, an attempt has been made to construct an energy diagram for DISA in a proton transfer cycle. Applying Eq. (2) the average $S'_1 \rightarrow S'_0$ and $T'_1 \rightarrow S'_0$ gaps were deduced to be 18 034 and 13 985 cm^{-1} , respectively. Conversely, the absorption maximum of 360 nm (27 778 cm^{-1}) was adopted for the S_1 state. The T_1 state of the enol conformer (E) is not available due to its negligible population efficiency. Alternatively, the average phosphorescence frequency (21 357 cm^{-1}) of the E' conformer was taken to be the normal T_1 state. Finally, the relative energy between conformers E and K in the ground-state is experimentally inaccessible, and has to be obtained through the theoretical approach. The large spin-orbit-coupling factor limits precise ab initio calculations at higher-level basis sets. Alternatively, a semi-empirical PM3 method was performed, estimating the S'_0 state to be higher in energy than S_0 by 13.67 kcal/mol. Accordingly, relative energy levels for an overall proton transfer cycle in DISA are depicted in Scheme 1. The $S_1 \rightarrow S'_1$ tautomerism is thermally allowed by ~ 14.2 kcal/mol. The T_1 state of the enol form is estimated to be ~ 7.4 kcal/mol higher in energy than the T'_1 state of the keto-tautomer. This value has to be treated as an upper limit since T_1 of the HB conformer E is in general lower in energy than that of the non-HB conformer E' , resulting in a reduction of the T_1 – T'_1 gap.

In conclusion, we have applied internal heavy-atom effects and an ultrasensitive near-IR detecting system to study the energetics and dynamics of the low-lying triplet states for ESIPT molecules. TRTL was proven to be a direct, feasible method to obtain the yield of the triplet state, and consequently the radiative decay rate can be extracted. The results lead to the establishment of relative energy levels for an overall proton-transfer cycle of DISA in different spin manifolds. While the occurrence of proton transfer has been widely accepted in the $^1\pi\pi^*$ state [1–5], it has been proposed that hydrogen-atom rather than proton transfer takes place in the triplet states [5,14,15,30]. Thus, whether the triplet-state hydrogen-atom transfer is operative and can be generalized in other systems

is of fundamental importance. For DISA the study of $T'_1 \rightarrow T_1$ tautomerism is not feasible due to the highly endergonic process. Further approach aimed at designing ESIPT molecules so that both dynamics and thermodynamics of the $T'_1 \rightarrow T_1$ tautomerism are accessible is in progress.

References

- [1] E.M. Kosower, D. Huppert, *Annu. Rev. Phys. Chem.* 37 (1986) 127.
- [2] Special Issue (P.F. Barbara, H.D. Trommsdorff (Eds.), *Spectroscopy and Dynamics of Elementary Proton Transfer in Polyatomic systems*), *Chem. Phys.* 136 (1989) 153.
- [3] S.F. Formosinho, L.G. Arnaut, *J. Photochem. Photobiol. A Chem.* 75 (1993) 21.
- [4] A. Douhal, F. Lahmani, A.H. Zewail, *Chem. Phys.* 207 (1996) 477.
- [5] S. Scheiner, *J. Phys. Chem. A* 104 (2000) 5898.
- [6] F. Parsapour, D.F. Kelley, *J. Phys. Chem.* 100 (1996) 2791.
- [7] A. Sytnik, M. Kasha, *Proc. Natl. Acad. Sci. USA* 91 (1994) 8627.
- [8] P.T. Chou, D. McMorro, T.J. Aartsma, M. Kasha, *J. Phys. Chem.* 88 (1984) 4596.
- [9] A.V. Acuna, F. Amat-Guerri, J. Catalán, A. Costella, J. Figuera, J. Munoz, *Chem. Phys. Lett.* 132 (1986) 576.
- [10] J. Catalán, J.C. del Valle, R.M. Claramunt, D. Sanz, J. Dotor, *J. Lumin.* 68 (1996) 165.
- [11] A.D. Roshal, A.V. Grigorovich, A.O. Doroshenko, V.G. Pivovarenko, *J. Phys. Chem. A* 102 (1998) 5907.
- [12] C.L. Renschler, L.A. Harrah, *Nucl. Inst. Methods Phys. Rev., A* 235, Sept., U.S. Patent, 1985, 635.
- [13] A.Z. Weller, *Elektrochemie* 60 (1956) 1144.
- [14] M.F.R. Prieto, B. Nickel, K.H. Grellmann, A. Mordzinski, *Chem. Phys. Lett.* 146 (1988) 387.
- [15] K.H. Grellmann, A. Mordzinski, A. Heinrich, *Chem. Phys.* 136 (1989) 201.
- [16] P.T. Chou, S.L. Studer, M.L. Martinez, *Chem. Phys. Lett.* 178 (1991) 393.
- [17] A. Grabowska, P. Borowicz, D.O. Martire, S.E. Braslavsky, *Chem. Phys. Lett.* 185 (1991) 206.
- [18] J. Catalán, C. Diaz, *J. Phys. Chem. A* 102 (1998) 323.
- [19] S.P. McGlynn, T. Azumi, M. Kinoshita, in: *Molecular Spectroscopy of the Triplet State*, Prentice Hall, Englewood Cliffs, NJ, 1969, p. 18.
- [20] W. Sieband, *J. Chem. Phys.* 47 (1967) 2411.
- [21] W. Klöpffer, *Adv. Photochem.* 10 (1977) 311.
- [22] P.T. Chou, G.R. Wu, Y.I. Liu, W.S. Yu, C.S. Chiou, *J. Phys. Chem. A* 106 (2002) 5967.
- [23] S. Nagaoka, N. Hiorta, M. Sumitani, K. Yoshihara, *J. Am. Chem. Soc.* 105 (1983) 4220.
- [24] S. Nagaoka, U. Nagashima, N. Ohta, M. Fujita, T. Takemura, *J. Phys. Chem.* 92 (1988) 166.

- [25] M.A. Morgan, E. Orton, G.C. Pimentel, *J. Phys. Chem.* 94 (1990) 7927.
- [26] P.T. Chou, Y.C. Chen, W.S. Yu, Y.H. Chou, C.Y. Wei, Y.M. Chen, *J. Phys. Chem. A* 105 (2001) 1731.
- [27] For example, see: S.E. Braslavsky, K. Heihoff, *Handbook of Organic Photochemistry*, CRC Press, Boca Raton, FL, 1989.
- [28] This number is calculated from Stokes–Einstein equation, see: J.B. Birks, in: *Photophysics of Aromatic Molecules*, Wiley, New York, 1970, p. 313.
- [29] M. Čuma, S. Scheiner, T. Kar, *J. Am. Chem. Soc.* 120 (1998) 10497.
- [30] For example, see: T. Suzuki, T. Omori, T. Ichimura, *J. Phys. Chem. A* 101 (2000) 11671.